Amyloid Fibrils

DOI: 10.1002/anie.201108040

Detailed Analysis of the Energy Barriers for Amyloid Fibril Growth**

Alexander K. Buell, Anne Dhulesia, Duncan A. White, Tuomas P. J. Knowles, Christopher M. Dobson, and Mark E. Welland**

Solubility is a key requirement for the functioning of a protein within the complex network of cellular components.[1–4] A class of highly debilitating disorders, including Alzheimer's and Parkinson's diseases, is related to the loss of solubility of peptides and proteins that is accompanied by their aggregation into ordered amyloid fibrils.[5] It has been found that, under at least some physiological conditions, these aggregates are thermodynamically more stable than the native forms of biological polypeptides.[6] This finding raises questions as to the factors governing the crucial ability of native proteins to remain soluble even under conditions where they do not necessarily correspond to global minima on free energy landscapes. In order to address this question, we have studied in detail the kinetics of elongation of amyloid fibrils formed by a wide range of polypeptides. The formation of amyloid fibrils from soluble protein molecules involves at least a primary nucleation step, an elongation step and, in general, a secondary nucleation process such as fibril fragmentation.[7] In addition, multiple interconverting oligomeric intermediates can be involved.[8] Measurements of amyloid growth in bulk solution often reflect all of these processes, and it can therefore be extremely challenging to determine accurately the concentrations of the different species and the rate constants for the individual elementary steps.

In order to overcome these difficulties, surface-based sensing techniques, notably those based on quartz crystal microbalance (QCM) measurements, have been developed in recent years, by which the growth of a constant, surface-bound ensemble of fibrils can be monitored.[9–11] These methods make use of the fact that in the presence of preexisting fibrils, aggregation can be highly accelerated through seeding.[12] This seeding process corresponds to the elongation of existing fibrils and can be well described as diffusional motion over a single free energy barrier,[13] involving no intermediate species between monomeric and fibrillar peptide. The elongation of the fibrils is monitored through the increase in hydrodynamic mass bound to the quartz crystal, as the rate of change of the resonant frequency is proportional to the average elongation rate of the fibrils.[9] The opportunity to image the sensor surface enables an estimation of the surface density of fibrils, an important factor in the determination of the rate constants in this bimolecular reaction, the overall rate of which depends on both the concentration of soluble protein and the number of available fibril ends. In addition, the lengths of the fibrils before and after an experiment can be compared and therefore an independent measurement of the length increase can be made and used to calibrate the frequency response of the microbalance. The covalent irreversible attachment of the preformed fibrils to the sensor surface[14] and the subsequent passivation of the remaining surface, as well as the short duration of individual experiments, ensure that only fibril elongation is measured, and that primary and secondary nucleation events can be neglected; this selectivity is confirmed by the high reproducibility of the data obtained from QCM measurements.[15]

The starting point of a systematic study of the energy barriers that separate the soluble from the fibrillar states of a protein is the measurement of the temperature dependence of the fibril elongation rate; such an approach allows for the determination of the enthalpy of activation from an Arrhenius plot. The temperature dependence of amyloid growth has already been measured for a range of amyloidogenic peptides and proteins,[16–22] and where possible these literature data are included in the analysis described herein. These published data have been acquired with a range of different techniques, mainly involving small-molecule labels such as Thioflavin-T. In such experiments, the exclusive study of the elementary elongation reaction is challenging and therefore the published values on energy barriers may in some cases refer to a combination of different elementary steps. We have, however, used the QCM approach, which is particularly suited for such measurements, to increase substantially the size of the available dataset by studying peptides and proteins of very diverse sequence that form amyloid fibrils under varied solution conditions. Figure 1 shows, as an example, raw QCM data for the temperature dependence of PI3K-SH3 amyloid fibril elongation, as well as AFM images of the QCM sensor surface.

Similar experiments were performed for a range of other peptides and proteins, and the resulting Arrhenius plots are shown in Figure 2. No pronounced curvature is apparent, unlike that sometimes observed for protein folding;[23] this

[*] A. K. Buell, M. E. Welland
Nanoscience Centre, University of Cambridge
11 JJ Thomson Avenue, West Cambridge CB3 0FF (UK)
E-mail: mew10@cam.ac.uk
A. K. Buell, A. Dhulesia, D. A. White, T. P. J. Knowles, C. M. Dobson
Department of Chemistry, University of Cambridge
Lensfield Road, Cambridge CB2 1EW (UK)
E-mail: cmd44@cam.ac.uk

[**] A.K.B. thanks Magdalene College for support through a research fellowship. We acknowledge support from the Wellcome (C.M.D., T.P.J.K.) and Leverhulme (C.M.D.) Trusts. We thank Novonordisk, Denmark, for a generous gift of glucagon, Vittorio Bellotti for providing β2-microglobulin, and Sarah Perrett for supplying the Ure2p (from *Saccharomyces cerevisiae*) protein. We thank David Chandler for helpful discussions.

Supporting information for this article is available on the WWW under http://dx.doi.org/10.1002/anie.201108040.

may simply be due to the narrower temperature range investigated in the present study. In addition, however, this finding suggests that the differences in heat capacity between the soluble states of the proteins and the transition states for the elongation reaction, $\Delta C_p^{\neq}$, are small. The enthalpies of activation $\Delta H^{\neq}$ were therefore extracted directly from linear fits. The values obtained are listed in Table 1 and plotted as bars in Figure 3.

In order to determine the free energies of activation $\Delta G^{\neq}$, the absolute elongation rate r was also measured in each case at 25 °C, as $r = [M]\Gamma\exp(-\Delta G^{\neq})$, where $[M]$ is the concentration of monomeric protein and Γ is a kinetic prefactor that can be calculated from polymer theory on the basis of our simplified model for amyloid fibril growth.[13] This method is formally equivalent to the one outlined in Ref. [24] and also obviates long extrapolation of Arrhenius plots. The absolute aggregation rate was estimated in a relatively straightforward manner from the surface-based QCM technique used in this study as discussed above, (see for example, Figure 1 b). The mass sensitivity of the QCM instrument for amyloid elongation measurements was empirically calibrated (see the Supporting Information) as existing models that relate the frequency change to an addition of mass are not appropriate to describe the hydrodynamics of a fibril layer in contact with liquid.

We have determined the mass sensitivity coefficient to be $(5 \pm 4)\,\mathrm{ng\,Hz^{-1}}$ for all the systems in this study (additional mass of elongated fibrils per observed frequency change). Together with the total number of fibrils on the crystal (extrapolated from images of several independent regions of the sensor), we were able to obtain the average elongation rate per fibril. This value, in turn, allows us to compute the free energy of activation $\Delta G^{\neq}$ and, together with the enthalpies of activation from the Arrhenius plots, we obtain the entropies of activation $T\Delta S^{\neq}$.

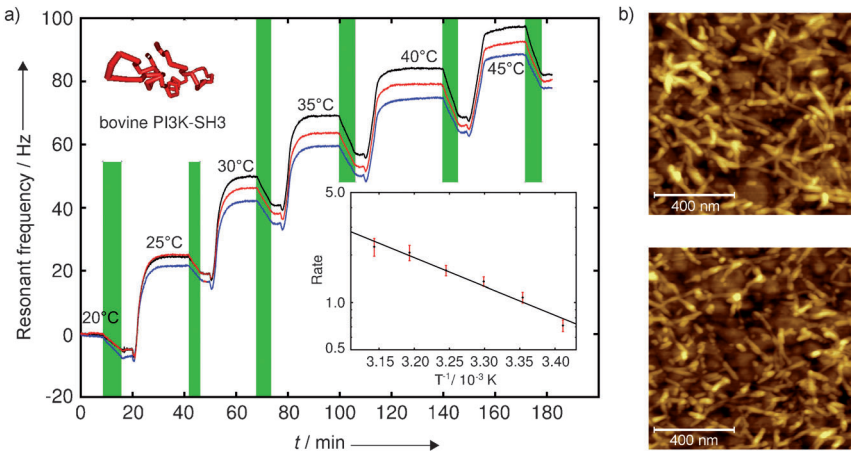

Figure 1. a) QCM experiments probing the temperature dependence of the elongation of PI3K-SH3 amyloid fibrils. The increase in temperature between each measurement leads to an increase in resonant frequency (white background). After a stable baseline had been established, the surface-bound fibrils were incubated in a solution of the same protein (green bands), and their elongation led to a decrease in resonant frequency due to the associated increase in surface-bound hydrodynamic mass. The rate of change of frequency is proportional to the (average) fibril elongation rate. The three frequency overtones $N = 3$ (black), $N = 5$ (red), and $N = 7$ (blue) are shown. The insert shows an Arrhenius plot of the raw data (the average of the three overtones is used). b) AFM images of two different areas of the QCM sensor used to estimate the surface number density of fibrils.

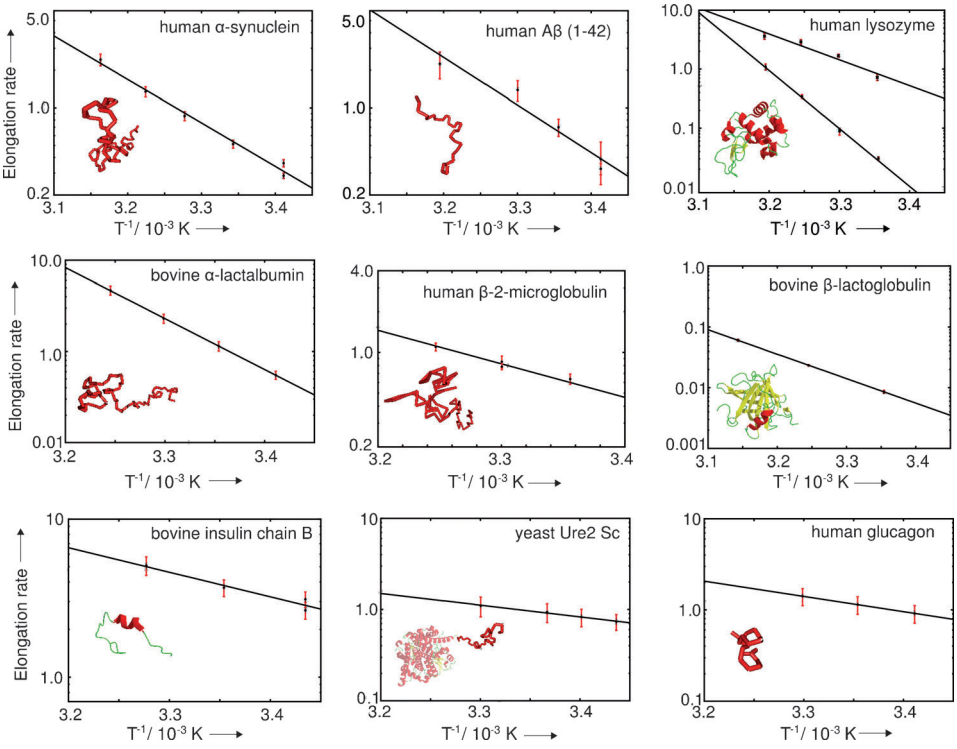

Figure 2. Arrhenius plots for the various peptides and proteins studied in this work. Each plot corresponds to a single experiment, similar to that shown in Figure 1. The error bars of the data points stem from the divergence of the frequency response for the overtones with N = 3, 5, 7 (see the Supporting Information for details). The molecules involved are illustrated schematically with pdb structures or random coils, as appropriate under the conditions of the experiment. For human lysozyme, two plots are shown, one corresponding to the native form of the protein (lower data points with steeper slope), and the other to the form where the disulfide bonds are reduced (see text and the Supporting Information).

Table 1: Summary of the thermodynamic parameters of activation determined for the proteins examined in this study, along with additional data taken from the literature.[a]

Peptide/Protein	No. of residues	Structure	pH	Charge	Ionic strength [M]	$\Delta G^{\ddagger}$ [kJ mol^{-1}]	$\Delta H^{\ddagger}$ [kJ mol^{-1}]	$T\Delta S^{\ddagger}$ [kJ mol^{-1}] (at 298 K)
human glucagon	29	nt	2.0	+5	0.03	16.2+4.5−1.5	30.0±12.0	13.8±18.0
bovine insulin B-chain	30	nt	2.0	+3	0.01	16.2+4.4−1.5	35.0±10.0	18.8±16.0
human Aβ (1–42)	42	nt	7.4	−3	0.1	5.9+4.0−1.4	66.1±8.1	60.2±13.5
bovine insulin	51	t	2.0	+5	0.01	25.0+4.0−1.5	102.5±4.2[9]	77.5±9.6
yeast Ure2p	354 (≈70)	nt	8.4	−7	0.25	9.6+4.0−1.5	27.0±10.0	17.4±15.5
bovine PI3K-SH3	84	nt	2.0	+12	0.01	20.4+3.9−1.5	42.1±8.5	21.8±13.9
human β2-microglobulin	100	nt	2.0	+18	0.04	16.7+5.2−1.5	48.3±8.6	31.6±15.3
bovine α-lactalbumin	123	nt	1.2	+17	0.2	13.5+4.1−1.4	107.0±10.0	93.5±15.6
human lysozym (native)	130	t	1.2	+21	0.2	25.0+4.0−1.5	167.7±14.7	142.7±20.1
human lysozym (reduced)	130	nt	1.2	+21	0.2	9.9+4.1−1.4	68±12	58.1±17.5
human α-synuclein	140	nt	7.4	−9	0.15	13.9+4.1−1.5	71.0±5.6[b]	57.1±11.2
bovine β-lactoglobulin	162	t	2.0	+21	0.2	31.8+3.9−1.4	83.7±9.6[c]	53.9±14.9
human Aβ (1–40)	40	nt	1.0	+7	0.1	n/a	95.4±4.6[16]	n/a
human Aβ (1–40)	40	nt	7.5	−4	0.15	n/a	61.9±1.3[27]	n/a
human Aβ (1–40)	40	nt	3.1	+6	0.1	n/a	42.9[19]	n/a
fungal Het-s	289 (≈70)	nt	7.0	−6	0.12	n/a	16±2[28]	n/a
human stefin B	98	t	4.75	+8	0.165	n/a	112.9±20.9[22]	n/a
human Ig light chain	122	t	7.4	+1	0.11	n/a	153±12[18]	n/a
human α-chymotrypsin	245	t	7.0	+4	0.15	n/a	208±17[21]	n/a

[a] We do not subtract the enthalpy of activation of water viscosity from the measured overall activation barrier, as is sometimes done in protein-folding studies.[29] In addition, we do not quote literature values for the entropy of activation, as this quantity is strongly model-dependent and difficult to compare between different studies. For Ure2p and Het-s, the number in brackets corresponds to the length of the fibril-forming domain. Abbreviations: nt = no tertiary structure, t = tertiary structure (see the Supporting Information for references). Where the enthalpies of activation have been reported previously, we find good agreement with our data. [b] (84.1±3.3) kJ mol^{-1} [17]. [c] 100.4 kJ mol^{-1}.[20]

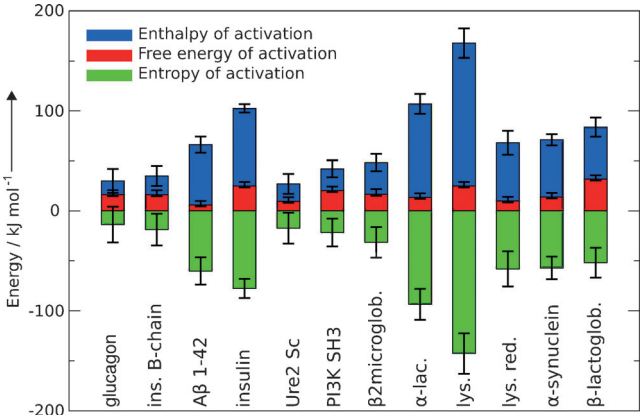

Figure 3. Overview of the measured and calculated values of the activation parameters. All values for the enthalpies of activation $\Delta H^{\ddagger}$ are unfavorable, while those for the entropies of activation $-T\Delta S^{\ddagger}$ are favorable. The enthalpy–entropy compensation discussed in the text is evident from this dataset.

We note here that the largest uncertainties in the values of all the thermodynamic parameters are associated with the entropy terms, as they contain the combined uncertainties of both the free energy and the enthalpy measurements.

A summary of these experimental data and calculations is given in Figure 3 and Table 1 with error bars defined from multiple experiments; most measurements of temperature dependences were performed at least in triplicate. In addition, and in general, the smaller the value of $\Delta H^{\ddagger}$, the larger the relative error, as a result of the weaker dependence of the elongation rate on temperature. The determinations of the absolute elongation rates were also performed at least in triplicate; here the errors are dominated by the order of magnitude uncertainty in the mass sensitivity coefficients, which are linearly related to the errors in the rates.

A striking feature of this collection of data is that the enthalpies of activation are unfavorable in all cases, whereas the entropies of activation are universally favorable. Both enthalpy and entropy values vary more strongly in absolute terms than the free energies of activation; therefore the well-known phenomenon of enthalpy–entropy compensation, a characteristic of many reactions in (aqueous) solution,[25,26] is clearly apparent.

Having established this data set, and combining it with the available data from the literature (Table 1), we can now examine the information contained within it by correlating the values of the activation parameters with characteristics of the polypeptides involved. A plot of the activation enthalpies $\Delta H^{\ddagger}$ against sequence length (Figure 4a) shows that these quantities are significantly correlated ($r^2 = 0.51$). This finding suggests a simple scaling of the energetics of the transition state with the size of the protein. It is also apparent from this plot, however, that the proteins which are folded to a significant degree (i.e. that possess a substantial degree of tertiary structure) under the conditions at which the aggregation data were measured have in most cases higher activation enthalpies for a given sequence length. When the values of $\Delta H^{\ddagger}$ are normalized for the number of residues and grouped according to the presence of tertiary structure (Figure 4b) it emerges that the presence of significant tertiary structure generally increases the enthalpy of activation per residue. We note here that the fact that all experiments have been performed under

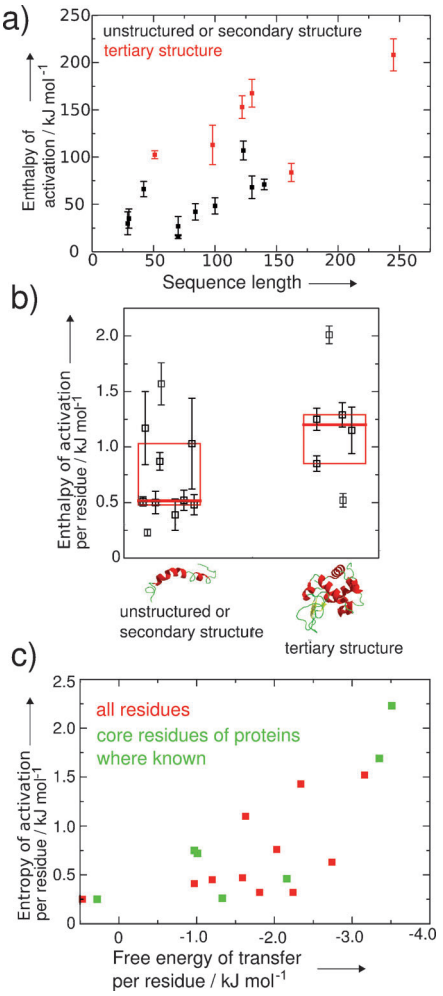

Figure 4. Correlations of the activation parameters with sequence properties of the polypeptides. a) Correlation of the enthalpy of activation for fibril elongation with sequence length ($r^2 = 0.51$). The data points are color coded according to whether the protein has significant native structure under amyloidogenic conditions (red, separate $r^2 = 0.41$) or not (black, separate $r^2 = 0.39$). b) The enthalpies of activation $\Delta H^{\ddagger}$ are shown divided by the number of residues. Box plots (red, showing median and upper and lower quartile) illustrate that a significant part of the enthalpy of activation is determined by the presence of tertiary structure in the soluble amyloidogenic protein (MannWhitney $U = 12.5$, $n_1 = 10$, $n_2 = 6$, $P = 0.066$ two-tailed). c) The entropy of activation per residue is plotted against the average hydrophobicity of the polypeptide (taken as the free energies of transfer from water to octanol, from Ref. [35]) (red points). The analysis is further refined by plotting only data for proteins for which an estimate of the regions of the sequence forming the fibril cores has been reported (see the Supporting Information). The correlation is better after the refining (r^2 changes from 0.37 to 0.71), indicating that hydrophobicity contributes significantly to the favorable entropy of activation.

solution conditions where the amyloidogenicity of the respective polypeptide is high is likely to reduce the observed correlation, as it is known that most of these conditions destabilize tertiary structure.[30]

Further support for the hypothesis that the presence of nonrandom structure, in addition to the number of residues, determines at least a part of the activation enthalpy for amyloid elongation is given by the observation that reduction and blocking of the disulfide bonds of human lysozyme results in a significant reduction (more than 50%) in the enthalpy of activation (see Figure 2 and Table 1). Reduction leads to the complete disappearance of all tertiary structure in lysozyme (see Ref. [31] and the Supporting Information). Despite the complex effects that disulfide cleavage can have on the overall energy landscape of a protein, this result further supports the hypothesis that the presence of tertiary structure contributes to the energy barrier for the conversion of the protein from the soluble to fibrillar state.

According to Figure 4a, however, a very large contribution to the activation enthalpy scales with the number of residues in the polypeptide. Therefore, the overall activation enthalpy is likely to be a sum of a large number of weak interactions, the number of which seems to be proportional to sequence length. When a polypeptide rearranges in an aqueous environment, large numbers of hydrogen bonds and other weak interactions are simultaneously broken and formed, often with very little net change in overall energy.[32] These energetic changes are, however, often accompanied by changes in the entropy of the system, especially for processes involving hydrogen bonds with water.[33] For example, when a monomeric polypeptide molecule incorporates into a fibril, it will expose less of its total surface area to the aqueous environment, and therefore the incorporation will be accompanied by (partial) desolvation, which results in both enthalpic and entropic changes. This process could therefore not only account for the correlation of Figure 4a, but also account for the favorable, and in some cases very large, entropies of activation[34] (Figure 3 and Table 1).

In order to probe this hypothesis further, we have plotted the average entropy of activation per residue against the average hydrophobicity of the respective sequence (Figure 4c); as a measure of the hydrophobicity, we use here the free energy of transfer from water to octanol of the amino acids (see Ref. [35] and the Supporting Information for details). These two quantities are weakly correlated ($r^2 = 0.37$) (red data points), but even if such a correlation were to be strong, it is unlikely to be easily detectable in our data set as the variability in the solution conditions and other contributions to the entropy of activation, such as losses of translational and chain entropy, are not taken into account in this analysis. However, in an attempt to explore a potential connection between hydrophobicity and entropy of activation more clearly, we have restricted the analysis to those polypeptides for which the region of the sequence that is likely to be primarily in the core of the amyloid fibril has been reported (see the Supporting Information); these regions of the sequence are likely to be more crucially involved in the formation of the transition-state ensemble than other parts of the peptide sequence. When the entropies of activation are divided by the number of "core" residues, the correlation with the average hydrophobicity of these specific residues is indeed stronger (green data points, $r^2 = 0.71$). This analysis strongly suggests that the desolvation of hydrophobic regions of the peptide sequence in the transition-state ensemble is a major contribution to the favorable activation entropy.

In summary, we have measured and analyzed the free energy barriers associated with the growth of amyloid fibrils using QCM techniques. We have found that the unfavorable enthalpies of activation, $\Delta H^{\ddagger}$, stem from the net unfavorable formation and breakage of many weak interactions necessary to reach the transition state ensemble of structures, presumably mainly between the polypeptide and the solvent water, and from the need to unfold residual structure that is associated with the soluble state of the protein. The entropies of activation, however, are favorable and we have found that this quantity correlates with the hydrophobicity of the core regions of the polypeptides that form the fibrils. This study therefore provides important information about the molecular origin of the energy barriers that are responsible in many cases for the metastability of soluble proteins against aggregation,[6] and therefore contributes to an understanding of the factors that govern the balance within proteins between normal function and aberrant behavior[36] leading to disease.

Experimental Section

The measurements of amyloid elongation kinetics were performed using an E4 quartz crystal microbalance (Q-Sense, Västra Frölunda, Sweden). The data analysis is described in detail in the Supporting Information. For the estimation of the surface concentration of fibrils, the QCM sensor surfaces were imaged in air before and/or after the kinetic experiments, using a Molecular Imaging PicoPlus (Tempe, AZ) atomic force microscope, and the fibrils within defined areas were counted. The proportionality factor between the frequency shift and the increase in protein mass was analyzed in detail and defined for four polypeptides (human Aβ (1–42), yeast Ure2p, human α-synuclein, and bovine insulin) by two different methods (peptide depletion and AFM length increase, see the Supporting Information).

Received: November 15, 2011
Revised: January 13, 2012
Published online: April 5, 2012

Keywords: amyloids · energy barriers · protein folding · quartz crystal microbalance

[1] C. H. Schein, *Biotechnology* **1990**, *8*, 308 – 317.
[2] C. M. Dobson, *Trends Biochem. Sci.* **1999**, *24*, 329 – 332.
[3] E. Gazit, *Angew. Chem.* **2002**, *114*, 267 – 269; *Angew. Chem. Int. Ed.* **2002**, *41*, 257 – 259.
[4] M. Vendruscolo, T. P. J. Knowles, C. M. Dobson, *Cold Spring Harbor Perspect. Biol.* **2011**, *3*(12), a010454.
[5] C. M. Dobson, *Nature* **2003**, *426*, 884 – 890.
[6] J. Baldwin, T. P. J. Knowles, G. G. Tartaglia, A. W. Fitzpatrick, G. L. Devlin, S. L. Shammas, C. A. Waudby, M. F. Mossuto, S. Meehan, S. L. Gras, J. Christodoulou, S. J. Anthony-Cahill, P. D. Barker, M. Vendruscolo, C. M. Dobson, *J. Am. Chem. Soc.* **2011**, *133*, 14160 – 14163.
[7] T. P. J. Knowles, C. A. Waudby, G. L. Devlin, S. I. A. Cohen, A. Aguzzi, M. Vendruscolo, E. M. Terentjev, M. E. Welland, C. M. Dobson, *Science* **2009**, *326*, 1533 – 1537.
[8] R. Kayed, E. Head, J. L. Thompson, T. M. McIntire, S. C. Milton, C. W. Cotman, C. G. Glabe, *Science* **2003**, *300*, 486 – 489.
[9] T. P. J. Knowles, W. Shu, G. L. Devlin, S. Meehan, S. Auer, C. M. Dobson, M. E. Welland, *Proc. Natl. Acad. Sci. USA* **2007**, *104*, 10016 – 10021.
[10] M. B. Hovgaard, M. Dong, D. E. Otzen, F. Besenbacher, *Biophys. J.* **2007**, *93*, 2162 – 2169.
[11] J. A. Kotarek, K. C. Johnson, M. A. Moss, *Anal. Biochem.* **2008**, *378*, 15 – 24.
[12] J. T. Jarrett, E. P. Berger, P. T. Lansbury, *Biochemistry* **1993**, *32*, 4693 – 4697.
[13] A. K. Buell, J. R. Blundell, C. M. Dobson, M. E. Welland, E. M. Terentjev, T. P. J. Knowles, *Phys. Rev. Lett.* **2010**, *104*, 228101.
[14] A. K. Buell, D. A. White, C. Meier, M. E. Welland, T. P. J. Knowles, C. M. Dobson, *J. Phys. Chem. B* **2010**, *114*, 10925 – 10938.
[15] D. A. White, A. K. Buell, C. M. Dobson, M. E. Welland, T. P. J. Knowles, *FEBS Lett.* **2009**, *583*, 2587 – 2592.
[16] Y. Kusumoto, A. Lomakin, D. B. Teplow, G. B. Benedek, *Proc. Natl. Acad. Sci. USA* **1998**, *95*, 12277 – 12282.
[17] V. N. Uversky, J. Li, A. L. Fink, *J. Biol. Chem.* **2001**, *276*, 10737 – 10744.
[18] Y.-S. Kim, T. W. Randolph, F. J. Stevens, J. F. Carpenter, *J. Biol. Chem.* **2002**, *277*, 27240 – 27246.
[19] R. Carrotta, M. Manno, D. Bulone, V. Martorana, P. L. S. Biagio, *J. Biol. Chem.* **2005**, *280*, 30001 – 30008.
[20] K. R. Domike, A. M. Donald, *Biomacromolecules* **2007**, *8*, 3930 – 3937.
[21] N. Rezaei-Ghaleh, A. Ebrahim-Habibi, A. A. Moosavi-Movahedi, M. Nemat-Gorgani, *Arch. Biochem. Biophys.* **2007**, *457*, 160 – 169.
[22] K. Škerget, A. Vilfan, M. Pompe-Novak, V. Turk, J. P. Waltho, D. Turk, E. Žerovnik, *Proteins Struct. Funct. Bioinf.* **2009**, *74*, 425 – 436.
[23] M. Oliveberg, Y. J. Tan, A. R. Fersht, *Proc. Natl. Acad. Sci. USA* **1995**, *92*, 8926 – 8929.
[24] R. Krug, W. Hunter, R. Grieger, *Nature* **1976**, *261*, 566 – 567.
[25] V. M. Krishnamurthy, B. R. Bohall, V. Semetey, G. M. Whitesides, *J. Am. Chem. Soc.* **2006**, *128*, 5802 – 5812.
[26] E. B. Starikov, B. Nordén, *J. Phys. Chem. B* **2007**, *111*, 14431 – 14435.
[27] K. Hasegawa, K. Ono, M. Yamada, H. Naiki, *Biochemistry* **2002**, *41*, 13489 – 13498.
[28] R. Sabaté, V. Castillo, A. Espargaro, S. J. Saupe, S. Ventura, *FEBS J.* **2009**, *276*, 5053 – 5064.
[29] B. Schuler, E. A. Lipman, W. A. Eaton, *Nature* **2002**, *419*, 743 – 747.
[30] A. K. Buell, A. Dhulesia, M. F. Mossuto, N. Cremades, J. R. Kumita, M. Dumoulin, M. E. Welland, T. P. J. Knowles, X. Salvatella, C. M. Dobson, *J. Am. Chem. Soc.* **2011**, *133*, 7737 – 7743.
[31] M. F. Mossuto, B. Bolognesi, B. Guixer, A. Dhulesia, F. Agostini, J. R. Kumita, G. G. Tartaglia, M. Dumoulin, C. M. Dobson, X. Salvatella, Angew. Chem. **2011**, *123, 7186 – 7189; Angew. Chem. Int. Ed.* **2011**, *50*, 7048 – 7051; *Angew. Chem. Int. Ed.* **2011**, *50*, 7048 – 7051.
[32] R. L. Baldwin, *J. Mol. Biol.* **2007**, *371*, 283 – 301.
[33] D. Chandler, *Nature* **2005**, *437*, 640 – 647.
[34] K. Lum, D. Chandler, J. D. Weeks, *J. Phys. Chem. B* **1999**, *103*, 4570 – 4577.
[35] J. Fauchere, V. Pliska, *Eur. J. Med. Chem.* **1983**, *18*, 369 – 375.
[36] A. W. Fitzpatrick, T. P. J. Knowles, C. A. Waudby, M. Vendruscolo, C. M. Dobson, *PLoS Comput. Biol.* **2011**, *7*, e1002169.

